Core Excitations of Biphenyl

I. Minkov,* F. Gel'mukhanov, and H. Ågren

Theoretical Chemistry, Roslagstullsbacken 15, Royal Institute of Technology, S-106 91 Stockholm, Sweden

R. Friedlein, C. Suess, and W. R. Salaneck

Department of Physics (IFM), Linköping University, S-581 83 Linköping, Sweden

Received: October 6, 2004; In Final Form: December 7, 2004

High-resolution C(1s) near-edge X-ray absorption and X-ray photoionization spectra of the free biphenyl molecule are presented and theoretically analyzed in order to allow an assignment of the observed spectral features. Finite lifetime broadening, a high density of vibrational states, and a strong overlap of contributions from chemically different carbon atom sites only partially allow resolving the vibrational fine structure. However, the shape and width of the spectral profiles are strongly determined by both chemical shifts and vibronic effects. In particular, different from photoionization of valence levels, both types of core level spectra do not contain contributions from dihedral modes which are related to the twisting motion of the two phenyl rings. Contrary to naphthalene, C−H stretching modes are significantly enhanced in the core excitation spectra of biphenyl while the contributions from C−C stretching modes are reduced.

Introduction

For several decades X-ray photoelectron (XPS) and near-edge X-ray absorption (NEXAFS) spectroscopies have been among the most important tools in probing the local electronic structure of matter.[1−3] In recent years the evolution of high-brilliance synchrotron radiation sources has extended the range of applications of monochromatic X-rays further. In particular, high spectral resolution[4] allows distinguishing even between minute core-level chemical shifts representing different atomic sites and individual vibrational levels.[5] In polyatomic organic molecules these chemical shifts are often small (∼0.1−1 eV), comparable to vibrational excitation energies and lifetime broadening.

The influence of the electronic environment of individual atoms (chemical shift) and of the nuclear dynamics accompanying the excitation process (vibrational excitations) can in many cases now be recognized in the shape of the spectral features of core photoionization lines and NEXAFS spectra of polyatomic systems, where in the latter spectra they depend also on the unoccupied molecular orbital (MO) in which the electron is placed during the core excitation process. In some rare cases[5−7] even vibrational fine structure can be resolved. Vibronic and chemical effects have been recognized or discussed for the NEXAFS spectra of a number of organic molecules such as formaldehyde,[8,9] alkanes,[10−12] benzene,[13] chloromethanes, and some monosubstituted benzenes,[9] polyenes,[14] polystyrene isotopomers,[15] and naphthalene.[5]

Because of the large number of degrees of freedom in such systems, it appears that ab initio simulations are a suitable way to properly describe the XPS and NEXAFS profiles and analyze the role of different mechanisms in the formation of X-ray resonances. Recent advances in the experimental techniques[16] also call for a constant refinement of the theoretical models[5,17] used to simulate NEXAFS and XPS spectra.

* To whom correspondence should be addressed. E-mail: ivo@theochem.kth.se.

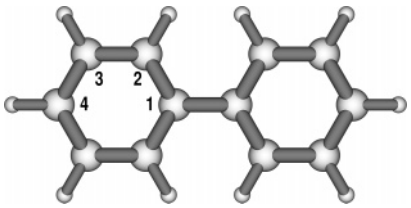

Figure 1. Biphenyl molecule and its chemically different atomic sites.

In this article high-resolution experimental and simulated C(1s) XPS and NEXAFS spectra of the free biphenyl molecule (Figure 1) are presented. This molecule is a model system for an important family of conjugated polymers, the poly-*p*-phenylenes (PPPs) and poly-dioctylfluorenes (PFOs), which are widely employed in organic electronic devices.[18,19] In PFO biphenyl constitutes the unit cell of the infinite polymer chain. By studying the biphenyl molecule with a high precision not achievable for polymers, access to specific electronic properties of the larger system (like the coupling of charges and excitations to vibrations/phonons) might be gained. To detect the influence of the molecular structure on the core excited state, results are compared to benzene[13,15,20] and naphthalene.[5] In the case of a weak coupling between the two aromatic rings one might expect a behavior similar to benzene. If the coupling is strong, like in naphthalene, on the other hand, major differences might occur.

Experimental Section

The measurements have been performed on beamline I411 at MAX-Lab in Lund, Sweden[5,21] on a stream of biphenyl molecules (Sigma-Aldrich Co., >99% purity) from a home-built, externally feedable Knudsen cell. The glass crucible was heated to 60 ± 20 °C, which lead to a maximal pressure in the chamber of about 3×10^{-6} mbar and moderate temperatures in the target zone.

The spectra were recorded with the Scienta SES-200 photoelectron spectrometer at the magic angle (54.7°) between the

10.1021/jp045447z CCC: $30.25
Published on Web 02/02/2005

electric field vector of the light and the direction of the electron emission. The near-edge X-ray absorption fine structure spectrum was measured using the Auger yield technique (kinetic-energy window between 240 and 274 eV) and normalized to the incoming photon flux. The (total) energy resolution was 75 meV for the C(1s) XPS line measured with 350-eV photons, about 50−60 meV for the high-resolution carbon K-edge NEXAFS spectrum measured in a narrow energy range and about 150 meV for the NEXAFS spectrum in a wider energy range. The photon and kinetic energies of the electrons were calibrated from the position of the Ar(2p) line excited by first- and second-order light. The uncertainty of the photon and electron energies is estimated to about 100 meV. Further experimental details are given elsewhere.[5]

Theory

For simulation of the photoionization and absorption spectra we used a theoretical framework outlined elsewhere.[5,9] The cross-section of the studied processes is calculated from the expression

$$\sigma(\omega) = \sum_{e,n} f_{0e} V \prod_{\alpha} \langle 0|n_\alpha\rangle^2 \qquad (1)$$

where f_{0e} is the oscillator strength and $\langle 0|n_\alpha\rangle^2$ represents the Franck−Condon (FC) factor of the transition from the ground state to the nth vibrational level of mode α in the excited state; the summation runs over the electronic and vibrational states. The shape of the electron−vibrational transition profile was approximated by a Voigt profile

$$V = \int_{-\infty}^{+\infty} d\epsilon \frac{e^{-\epsilon^2/\gamma^2}}{\gamma\sqrt{\pi}} \Delta\left(\Omega - \epsilon, \frac{\Gamma_L}{2}\right) \qquad (2)$$

which is the convolution of a Lorentzian function with full-width at half-maximum (fwhm) Γ_L and a Gaussian function with fwhm Γ_G. Here, we use atomic units and the following notations: $\gamma = \Gamma_G/2\sqrt{\ln 2}$; $\Delta(\Omega,\Gamma_L/2) = \Gamma_L/[2\pi(\Omega^2 + \Gamma_L{}^2/4)]$, where $\Omega = BE - \omega_{f0}$ and $\Omega = \omega - \omega_{f0}$ for XPS and NEXAFS, respectively. The binding energy, $BE = \omega - E$, is the difference between the photon frequency, ω, and the photoelectron energy, E; ω_{f0} is the resonant frequency of the electron−vibrational transition $0 \rightarrow f$.

In our calculations we used a lifetime broadening of the carbon core excited states $\Gamma_L = 100$ meV.[22] Instrumental broadening was chosen according to the experimental resolution: $\Gamma_G = 55$ (fwhm) and 75 meV (fwhm) for the high-resolution NEXAFS and XPS spectra, respectively.

Calculations of the excitation energies and oscillator strengths have been performed using the DFT-based transition potential method.[23] This technique is particularly suitable for description of photoionization and photoexcitation processes as it accounts for relaxation and dynamical correlation effects[24] which are known to be important for correct treatment of core excited systems. Furthermore, it shows superior performance as compared to other methods (Z + 1 method, ΔSCF, etc.). To account for core−hole relaxation effects, we made use of the double-basis set technique.[25]

The geometry of the molecule was optimized at the B3LYP/aug-cc-pVDZ level using the *Gaussian 03* package.[29] Calculation of vibrational frequencies was performed employing the cc-pVDZ basis set and the CASSCF method ([12,12] active space) which is implemented in the Dalton program package.[30] As performed previously,[5] we use a numerical differentiation technique in order to obtain the excited-state potential-energy surface gradients at the ground-state geometry, $\Delta E_{exc}/\Delta Q_\alpha$, where ΔQ_α is the deviation of the normal coordinate from the ground-state geometry.[31] These gradients then serve as input for the calculation of Franck−Condon factors.

The nuclear dynamics during the excitation process is evaluated in a model[26] which neglects the vibrational coupling (VC) between core excited states. The VC can be important if the core excited states are close in energy. One of the important effects resulting from VC is related to the dynamical core−hole localization.[27] In our simulations this effect is approximately accounted for by forcing the core−hole to be localized. Since this approach is an approximation, some differences between the simulated and experimental spectra can be attributed to these restrictions of our model.

The postcollisional interaction (PCI) is neglected in calculation of the XPS spectrum, since for high kinetic energies of the photoelectron (of about 60 eV in the experiment) the PCI is usually small.[28]

TABLE 1: Calculated Vertical and Experimental (XPS maximum peak position, (Figure 2)) C(1s) Binding Energies for the Four Symmetrically Distinguishable Carbon Atoms in Biphenyl

	C1	C2	C3	C4	exptl
BE (eV)	289.301	288.937	289.100	288.962	290.0

TABLE 2: Franck−Condon Factors for the Strongest Vibrational Modes C(1s) Photoionization: XPS

				FC factors		
site	mode	ω (eV)	symmetry	$\langle 0\|0\rangle^2$	$\langle 0\|1\rangle^2$	$\langle 0\|2\rangle^2$
	21	0.173	B2	0.916	0.080	0.003
	29	0.139	B1	0.897	0.098	0.005
C1	33	0.133	A	0.943	0.055	0.002
	35	0.129	B1	0.890	0.103	0.006
	44	0.098	B3	0.898	0.097	0.005
	3	0.407	B3	0.935	0.063	0.002
	5	0.406	A	0.912	0.084	0.004
C2	27	0.146	B2	0.926	0.071	0.003
	33	0.133	A	0.895	0.099	0.006
	35	0.129	B1	0.867	0.123	0.009
	44	0.098	B3	0.931	0.067	0.002
	7	0.404	B3	0.915	0.081	0.004
	9	0.403	B1	0.933	0.065	0.002
	27	0.146	B2	0.879	0.113	0.007
C3	31	0.137	A	0.782	0.192	0.024
	35	0.129	B1	0.909	0.086	0.004
	47	0.084	B1	0.865	0.125	0.009
	48	0.082	B2	0.937	0.061	0.002
	29	0.139	B1	0.851	0.137	0.011
	31	0.137	A	0.764	0.206	0.028
C4	33	0.133	A	0.915	0.081	0.004
	34	0.132	B1	0.945	0.054	0.002
	35	0.129	B1	0.915	0.081	0.004
	53	0.054	B1	0.938	0.060	0.002

Results and Discussion

Geometry of the Core Excited State. The phenyl rings in the biphenyl molecule can rotate fairly easily with respect to each other, experiencing only small energy barriers.[32,33] Electron diffraction data are consistent with a value for the dihedral angle of about 44.4° ± 1.2°.[34,35] In our calculations we obtain an angle of 38.8° in the ground state. It is interesting to see how the theoretical NEXAFS and XPS spectra will be influenced by this twist. In Table 3 are presented the 1s → LUMO X-ray absorption energies as well as oscillator strengths obtained for the optimized ground-state geometry and for the molecule in a planar conformation. It appears that both the transition energies

TABLE 3: Vertical C(1s → LUMO) Excitation Energies and Oscillator Strengths (NEXAFS) for Two Values of the Dihedral Angle between the Phenyl Rings (38.8° (optimized geometry) and 0.0° (planar geometry))

	dihedral	C1	C2	C3	C4
$E_{exc} - E_0$	38.8°	284.265	284.045	284.204	284.055
f		0.0166	0.0155	0.0169	0.0149
$E_{exc} - E_0$	0.0°	284.281	284.034	284.275	284.051
f		0.0152	0.0144	0.0167	0.0135

and strengths are very similar for the two angles, indicating that the X-ray absorption spectrum basically does not depend on how the rings are twisted. This is different from transitions between valence levels as discussed for the optical absorption spectra.[36]

In the case that the excited-state potential-energy surface of a molecular system is only slightly displaced from the ground-state geometry, vertical excitations reach only low vibrational levels. The harmonic approximation is then sufficiently accurate. We find that excitations beyond the third vibrational level of the excited states in biphenyl are small. This is remarkable since the potential-energy surface gradient for some of the C−H stretching modes is quite high, indicating that the potential-energy surface itself is quite narrow and steep. For narrow potential surfaces, displacements favor excitations of higher vibrational levels.

XPS. The simulated and experimental C(1s) photoelectron spectra are shown in Figure 2. The C(1s) line peaks at about 290.0 eV and is asymmetric, with a high-energy tail extending to about 291 eV. The overall shape is well reproduced by the calculations. The theoretical spectrum is shifted relative to the experimental one by about 1.1 eV toward lower energy, which is expected in the framework of the DFT-transition potential method.[23]

In Table 1 are presented the calculated C(1s) binding energies of all four chemically distinguishable atoms in the biphenyl molecule which are denoted C1, C2, C3, and C4. Interestingly, C1 and C3 have quite similar binding energies, and C2 and C4 do as well. The splitting between the two pairs is about 0.2 eV. The pairing of atoms is related to an alternation of the chemical environment for each atom, leading to the observed behavior of the chemical shifts. This alternating behavior is also a typical property of other aromatic systems and polyenes.[38,39]

The XPS profiles for all four carbon atoms (Figure 2) are determined by a rather broad spectral distribution of the FC factors. For the higher intensity transitions, they are listed in Table 2.

To evaluate the relative importance of contributions from individual carbon atoms and from vibrational modes we simulated the XPS profile with a very small lifetime broadening as plotted in Figure 3.

For all carbon atoms the 0−0 transitions have the highest intensity, with only small contributions from excitations to higher vibrational levels. Furthermore, only a small number of vibrational modes are excited. These modes are quite similar for C1, C2, C3, and C4: After the 0−0 line follows excitation of a low-energy bending (mode 44 and 47) or out-of-plane C−C mode (mode 53), then several C−C−H in-plane bending modes (modes 27, 29, 31, and 33) and a breathing mode (mode 35), and finally contributions from C−H stretching modes (modes 3, 5, 7, and 9). The latter provide a substantial contribution to the high binding energy tail of the spectrum, since even the second vibrational level is excited. C−C stretching modes are of less importance for the XPS spectrum. Contributions from vibrational modes related to the twisting motion are virtually

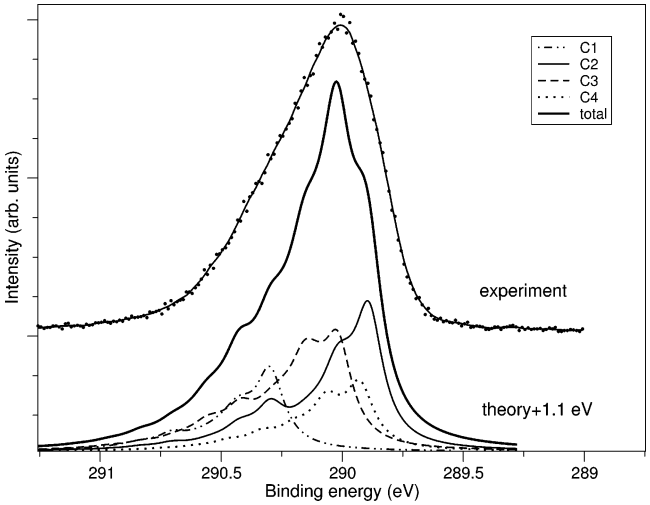

Figure 2. Calculated and experimental C(1s) photoelectron spectra of biphenyl: Γ_L(fwhm) = 100 eV, Γ_G(fwhm) = 75 meV. The theoretical profile is shifted by 1.1 eV toward higher energy in order to facilitate comparison with the experiment.

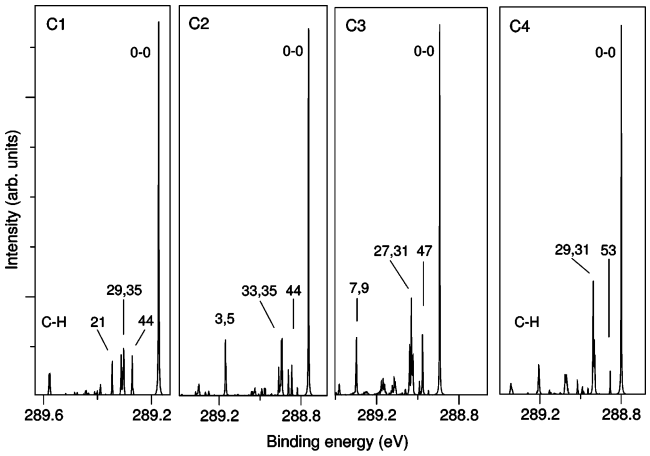

Figure 3. Vibrational resonances of the XPS for the four atomic sites with lifetime broadening $\Gamma_L = 5 \times 10^{-4}$ eV and $\Gamma_G = 0$. Modes 3, 5, 7, and 9 represent C−H stretches.

absent (in the case of C(1s) ionization as well as for X-ray absorption). Since the core excited-state energies also depend only weakly on the dihedral angle, as already mentioned, it is concluded that the biphenyl molecule retains its structure upon core ionization. Note that this is different for photoionization in the valence region. For example, upon ionization of the highest occupied molecular orbital (HOMO), the dihedral angle changes to a value of about 20°.[40] The vibrational spectrum of the resulting radical cation differs substantially from that of the neutral species.[40]

Summing up the contributions from all the atoms leads to the simulated XPS spectrum shown in Figure 2. In this case the high density of vibrational states and the strong overlap of the four atomic contributions does not allow resolving individual vibrational peaks anymore.

A comparison between naphthalene, analyzed in our previous work,[5] biphenyl, and benzene[20] provides information on how dynamic relaxation mechanisms accompanying core excitations depend on the way aromatic rings are fused: In naphthalene, the XPS line related to the bridging carbon atoms is separated by about 0.6 eV from the lines of the other carbon atoms. Such a large chemical shift is not observed in the biphenyl case where the shifts of about 0.2 eV are rather small and in benzene where the carbon atoms are chemically equivalent.

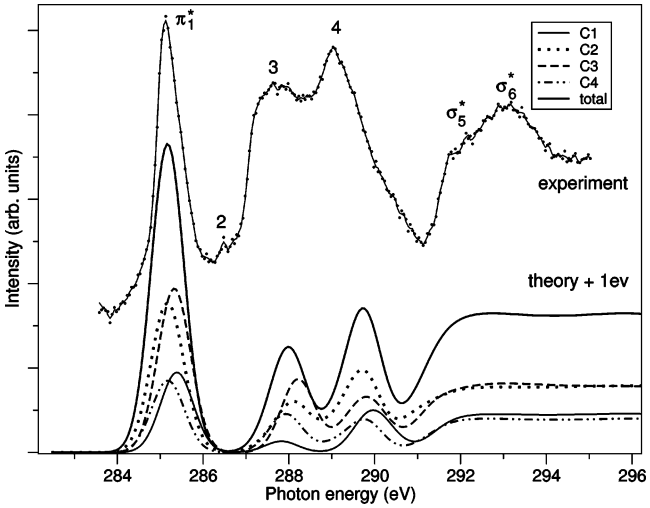

Figure 4. Experimental and theoretical NEXAFS in a wider energy range, from 284 to 295 eV. The theoretical profile contains only the electronic contribution from each of the four carbon centers and is broadened by a Lorentzian with $\Gamma = 0.90$ eV (fwhm) in order to reproduce the experimental width of the bands. It is also shifted by 1 eV toward higher photon energy.

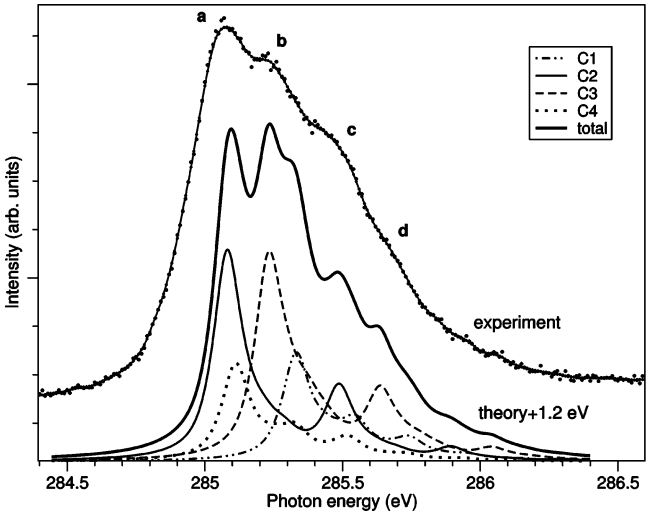

Figure 5. Calculated and experimental C(1s) absorption spectrum of biphenyl: NEXAFS: Γ_L(fwhm) = 100 eV, Γ_G(fwhm) = 55 meV. The theoretical profile is shifted by 1.2 eV toward higher photon energy Also, the individual atom contributions to the theoretical spectrum are presented.

The vibrational modes excited upon C(1s) photoionization are quite similar to those in benzene, where particularly C−H in-plane bending modes are strong. C−H stretching modes contribute to a minor extent. Note, however, that C−C stretching modes are stronger in benzene. For naphthalene, such C−C modes are even more pronounced than in benzene and C−H stretching modes are of even less importance.[5]

Both electronic (chemical shift) and nuclear (vibronic fine structure) relaxation mechanisms in biphenyl resemble those in benzene. This similarity leads to the conclusion that the phenyl rings largely keep their benzene character in the core excited state.

NEXAFS. The (low-resolution) carbon K-edge X-ray absorption spectrum in a wide energy region is shown in Figure 4. It is dominated by a ca. 0.7 eV broad, strong, and asymmetric π^* resonance peaking at about 285.07 eV, denoted π_1^*, followed by resonances 2, 3, and 4 at about 286.6, 287.6, and 289.0 eV, and the C−C σ^* resonances at about 291.9 and 293.1 eV, denoted σ_5^* and σ_6^*. Structures 2−4 might have contributions due to core excitations into π^* and C−H σ^* states.

It should be noted that the theoretical profile consists of only electronic contributions and is shifted by 1 eV toward higher energy in order to match the experimental curve. The shape and spacing of the peaks are well reproduced. However, the theoretical spectrum suffers from some lack of intensity.

The first prominent peak, π_1^*, is due to core excitations into the LUMO and very small contributions from transitions into the LUMO+1. The intensity of the former is much larger due to the excitonic character of the core excited state:[41] while there is still some resemblance to the LUMO and LUMO+1 orbitals of the ground state, both with e_{2u} symmetry, the symmetry is broken in the core excited state. In the system with a core−hole, the unoccupied orbitals are largely localized on only one of the phenyl groups.

However, due to the intrinsic asymmetry of the core−hole system, higher unoccupied orbitals completely lose their symmetry, and therefore, it is not possible to trace exactly their origin to the ground-state orbitals. Moreover, the unoccupied orbitals are preferably localized at one of the phenyl rings.

Peak 3 at about 287.9 eV is due to a group of excitations to LUMO+3, LUMO+4, and LUMO+5 with a dominant contribution from the latter two. The first one is still of π^* character, but the rest have pronounced C−H σ^* character. Thus, in this case, there are two types of overlapping excitations. Peak 4 at about 289.6 eV is mainly due to 1s transitions to several diffuse orbitals, which nevertheless have considerable p-electron density at the core excited site. The broad shape resonance in the continuum region of the spectrum is not well described. This could be attributed to the inherent difficulties of describing interactions with the continuum using a discrete and local basis set.

The picture sketched above resembles the benzene case,[39] taking into account the doubling of the system. The first π^* resonance is strongest, followed by a small second one. At higher energies two σ^*-type resonances appear with considerable CH character.

The carbon K-edge X-ray absorption spectrum in the region of the absorption threshold is shown in greater detail in Figure 5. Interestingly, the π_1^* resonance exhibits a fine structure, displaying shoulders **b** at 285.24 ± 0.01 eV, **c** at 285.49 ± 0.02 eV, and **d** at ca. 285.67 ± 0.03 eV, that is at the high-energy side of the first, well-defined peak **a** at 285.07 ± 0.01 eV. With an energetic progression of 170−250 meV, such structures are reminiscent of vibrational fine structure, possibly due to C−C in-plane stretching modes[5] or related to a chemical shift between different atomic sites.

The simulated spectrum shown in Figure 5 reproduces the overall width of the resonance and the high-energy tail. To resolve the nature of the X-ray absorption transitions contributing to this first resonance, the probability for possible electronic transitions forming the first NEXAFS band must be evaluated (Figure 5). In the ground state the energy separation between the lowest unoccupied molecular orbital (LUMO) and the next one, LUMO+1, both corresponding to the e_{2u} unoccupied orbitals in benzene, is about 0.56 eV. Upon core excitation the symmetry of these orbitals radically changes. Also, the LUMO−LUMO+1 separation rises to 1.1 eV in the core excited state. That is, the transition into the LUMO+1 overlaps energetically with the transition into the LUMO. Our simulations, however, show that the transition into the LUMO+1 is of several orders of magnitude lower intensity than that into the LUMO (Table 3) and thus does not contribute significantly to the spectrum.

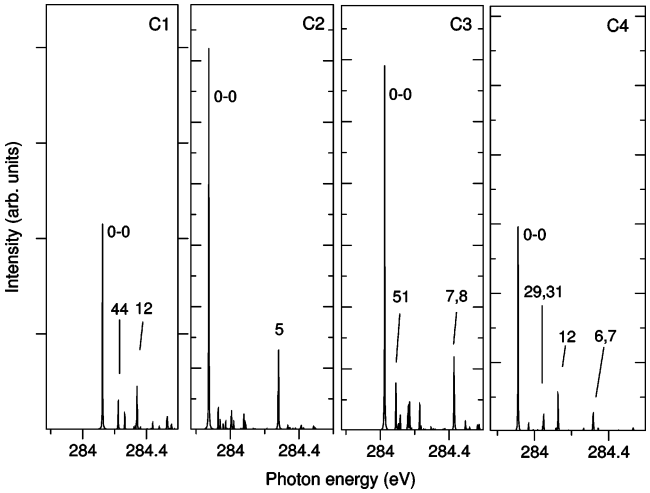

Figure 6. Vibrational resonances of the NEXAFS for the four atomic sites with lifetime broadening $\Gamma_L = 5 \times 10^{-4}$ eV and $\Gamma_G = 0$. Modes 5−8 represent C−H stretching modes.

The interaction with the core−hole removes the e_{2u} symmetry and leads to partial localization of several unoccupied orbitals. LUMO and LUMO+1 are partially localized at the ring where the core excitation occurs. However, at the core excited center LUMO+1 has a diminishing contribution, leading to a small transition dipole moment and a low transition probability. Finally, only C(1s) → LUMO transitions need to be discussed.

The double peak structure of the first resonance with a splitting of about 150 meV in the simulated NEXAFS spectrum, which is not so clearly observed in the experimental spectrum, has its origin in the contributions from individual atomic sites. The subspectra of the C1, C2, C3, and C4 atoms are also shown in Figure 5. Some peak structure in the high-energy tail arises from pronounced C−H stretching modes. As discussed in our previous work,[5] the present accuracy of ab initio methods used for the calculation of relative X-ray absorption energies is still challenging and cannot reproduce minute shifts of 100−200 meV. Another reason for discrepancies between experiment and simulations could be the neglect of the vibronic coupling between excited states. It is well known that in some cases vibronic interactions do play an important role in determining the shape of the spectra.[42−44]

The oscillator strengths for the C(1s) → LUMO electronic transitions (Table 3) are quite similar for all atomic sites. Because there are twice the number of atoms, the spectral intensity for C2 and C3 sites is double than that for the C1 and C4 sites. As for XPS, C1 and C3 have quite similar electronic excitation energies. The same is true for C2 and C4, which eventually leads to the double structure in the simulated spectrum.

The distribution of FC factors and therefore of the vibrational structure for each atomic contribution, plotted in Figure 6, is very similar to that in the XPS spectrum (compare Tables 2 and 4). The 0−0 line is again the dominating one, followed by moderate contributions from low-energy bending C−C modes (numbers 44 and 51) and C−H stretching modes (5−8) in the high-energy tail of the spectrum. C1 and C4 excitations couple additionally to a C−C stretching mode (number 12). At the C2 and C3 sites high contributions from C−H stretching modes are present. The highest energy part of the spectrum arises from excitations to the second vibrational level.

On the basis of these theoretical data an explanation of the observed experimental π_1^* fine structure can now be proposed:

TABLE 4: Franck−Condon Factors for the Strongest Vibrational Modes C(1s → LUMO) Photoabsorption: NEXAFS

				FC factors		
site	mode	ω (eV)	symmetry	$\langle 0\|0\rangle^2$	$\langle 0\|1\rangle^2$	$\langle 0\|2\rangle^2$
C1	11	0.218	B2	0.922	0.075	0.003
	12	0.216	A	0.822	0.161	0.016
	29	0.139	B1	0.931	0.067	0.002
	44	0.098	B3	0.871	0.120	0.008
C2	3	0.407	B3	0.914	0.083	0.004
	5	0.406	A	0.882	0.111	0.007
	8	0.404	B2	0.943	0.055	0.002
	14	0.205	B2	0.959	0.040	0.001
	33	0.133	A	0.953	0.046	0.001
	53	0.054	B1	0.948	0.051	0.001
C3	7	0.404	B3	0.881	0.112	0.007
	9	0.403	B1	0.921	0.075	0.003
	14	0.205	B2	0.935	0.063	0.002
	27	0.146	B2	0.925	0.072	0.003
	31	0.137	A	0.945	0.054	0.002
	51	0.066		0.878	0.115	0.008
C4	6	0.405	B1	0.943	0.055	0.001
	7	0.404	B3	0.976	0.023	0.000
	11	0.218	B2	0.922	0.075	0.003
	12	0.216	A	0.843	0.144	0.012
	29	0.139	B1	0.953	0.046	0.001
	31	0.137	A	0.936	0.061	0.002

The two high-energy shoulders **c** and **d** are most likely due to the first excited vibrational level of the C−H stretching modes at the C2 and C3 sites. In this case the 0−0 lines are expected to appear 404−406 meV lower in energy. This is, within the error bars, exactly where features **a** and **b** are. We therefore assign **a** and **b** to correspond essentially to the electronic excitations at the C2 and C3 sites, respectively, possibly slightly displaced due to overlapping contributions from the C1 and C4 sites.

The vibrational spectra for each pair, C1 and C4 as well as C2 and C3, are almost the same (Figures 5 and 6). This behavior can be understood by considering the positions of the atomic sites in the molecule: the C2 and C3 atoms are at the ortho and meta positions, respectively, while the C1 and C4 atoms are located at the molecular axis, at the para positions, in a notation commonly used for conjugated molecules. Obviously, upon fusing two benzene rings the vibrational coupling at the different sites becomes distinguishable: Excitations at the para positions (C1 and C4) are accompanied by a C−C stretch along the axis (mode 12), while at the C2 and C3 sites the benzene character[13,46] of the core excitations is maintained with a relatively high contribution from C−H stretching mode[45] (see Figure 6).

As compared to naphthalene,[5] in biphenyl C−H modes give a considerably larger contribution to the X-ray absorption spectra. The C−C stretching modes, mostly responsible for forming the naphthalene vibrational profile, are strongly reduced in biphenyl and contribute only with a single mode at the C1 and C4 sites (mode 12). Generally, the vibrational structure of all excited centers in biphenyl is less pronounced. Like the XPS spectrum, with the large chemical shift for the bridging atoms in naphthalene, the overall profile of the first π^* resonance is very different in naphthalene compared with biphenyl.

Conclusions

The high-resolution core-level photoionization and X-ray absorption spectra of free biphenyl molecules have been measured, analyzed, and compared to those of benzene and naphthalene. The spectral profiles are determined by the

interplay between chemical shifts and the vibrational fine structure. In the biphenyl case a finite lifetime broadening, a high density of vibrational states, and a significant overlap of the contributions from the four chemically shifted atomic sites only partially allow the experimental resolution of vibrational fine structure. Theoretical analysis provides an interpretation of the observed spectral profiles of the C(1s) XPS line and the first π^* resonance in the NEXAFS spectrum, and an assignment of shoulders at the high-energy tail in the absorption spectrum could be proposed.

For all chemically distinguishable atomic sites very few and similar modes are excited upon core excitation: For both XPS and NEXAFS, after the strong 0−0 excitation, there are excitations to low-energy bending or out-of-plane C−C modes, then several C−H and C−C bending modes, and finally contributions from C−H stretching modes. Only in the NEXAFS the latter are substantial, and even excitations to their second vibrational level occur, causing the long tails of the spectra. However, with respect to the vibrational excitations it is important which atomic site is excited. Furthermore, it matters how the aromatic rings are fused: In biphenyl, a C−H stretching mode has a significant contribution mainly for the ortho positions, whereas in naphthalene this mode is strongly suppressed. On the other hand, a C−C stretching mode is only weakly active in the NEXAFS spectrum of biphenyl, while in naphthalene it constitutes a major contribution.

We found that both the XPS and NEXAFS spectra are only minorly influenced by contributions from dihedral or twisting modes. Therefore, the biphenyl molecule retains its rigidity upon core excitation or core ionization, as opposed to valence-shell ionization. The calculations reveal that electronic excitation energies are less affected by the size of the dihedral angle.

Knowledge of how the geometry of rather small (oligomeric) molecules influences core excitation spectra can be foreseen to lead to an understanding of the core excited states of conjugated polymers and, in particular, of the technologically relevant polymers of the PFO family. By resolving vibrational excitations accompanying electronic excitation, even the dynamics of excitations can be studied.

Acknowledgment. The authors thank M. Tchaplyguine (Uppsala University, Sweden) and W. Osikowicz and R. Murdey (Linköping University) for experimental help and L. Sæthre (University of Bergen, Norway) for fruitful discussions. This work was performed within the Center for Advanced Molecular Material (CAMM), funded by the Swedish Science Foundation (SSF) and additionally supported by the Swedish Research Council (VR) under contracts 12252003 and 12252020. In addition, research in Linköping is supported by a Research Training Network (LAMINATE, project no. 00135) and the EU-Growth project MAC-MES (project no. GRD-2000-30242).

References and Notes

(1) Bressler, C.; Chergui, M. *Chem. Rev.* **2004**, *104*, 1781.

(2) de Groot, F. *Chem. Rev.* **2001**, *101*, 1779.

(3) Kosugi, N. *J. Electron Spectrosc. Relat. Phenom.* **2004**, *137*−*40*, 335.

(4) Prince, K. C.; Vondracek, M.; Karvonen, J.; Coreno, M.; Camilloni, R.; Avaldi, L.; deSimone, M. *J. Electron Spectros. Relat. Phenom.* **1999**, *101*−*103*, 141.

(5) Minkov, I.; Gel'mukhanov, F.; Friedlein, R.; Osikowicz, W.; Suess, C.; Öhrwall, G.; Sorensen, S. L.; Braun, S.; Murdey, R.; Salaneck, W. R.; Ågren, H. *J. Chem. Phys.* **2004**, *121*, 5733.

(6) Feifel, R.; Andersson, M.; Öhrwall, G.; Sorensen, S. L.; Piancastelli, M. N.; Tchaplyguine, M.; Björneholm, O.; Karlsson, L.; Svensson, S. *Chem. Phys. Lett.* **2004**, *383*, 222.

(7) Trofimov, A. B.; Moskovskaya, T. E.; Gromov, E. V.; Köppel, H.; Schirmer, J. *Phys. Rev. A* **2001**, *64*, 22504.

(8) Remmers, G.; Domke, M.; Puschmann, A.; Mandel, T.; Xue, C.; Kaindl, G.; Hudson, E.; Shirley, D. A. *Phys. Rev. A* **1992**, *46*, 3935.

(9) Plashkevych, O.; Privalov, T.; Ågren, H.; Caravetta, V.; Ruud, K. *Chem. Phys.* **2000**, *260*, 11.

(10) Remmers, G.; Domke, M.; Kaindl, G. *Phys. Rev. A* **1993**, *47*, 3083.

(11) de Miranda, M. P.; Beswick, J. A.; Parent, P.; Laffon, C.; Tourillon, G. *J. Chem. Phys.* **1994**, *10*, 5500.

(12) Naves de Britto, A.; Svensson, S.; Correa, N.; Keane, M. P.; Ågren, H.; Sairanen, O.-P.; Kivimäki, A.; Aksela, S. *J. Electron Spectrosc. Relat. Phenom.* **1992**, *59*, 293.

(13) Ma, Y.; Sette, F.; Meigs, G.; Modesti, S.; Chen, C. T. *Phys. Rev. Lett.* **1989**, *63*, 2044.

(14) Privalov, T.; Plashkevych, O.; Gel'mukhanov, F.; Ågren, H. *J. Chem. Phys.* **2000**, *113*, 3734.

(15) Urquhart, S. G.; Ade, H.; Rafailovich, M.; Sokolov, J. S.; Zhang, Y. *Chem. Phys. Lett.* **2000**, *322*, 412.

(16) Hergenhahn, U. *J. Phys. B: At. Mol. Opt. Phys.* **2004**, *37*, R89.

(17) Köppel, H.; Domcke, W.; Cederbaum, L. S. *Adv. Chem. Phys.* **1984**, *57*, 59.

(18) Hide, F.; Daz-Garca, M. A.; Schwartz, B. J.; Andersson, M. R.; Pei, Q.; Heeger, A. J. *Science* **1996**, *273*, 1833.

(19) Bernius, M. T.; Inbasekaran, M.; O'Brien, J.; Wu, W. *Adv. Mater.* **2000**, *12*, 1737.

(20) Myrseth, V.; Børve, K. J.; Wiesner, K.; Bässler, M.; Svensson, S.; Sæthre, L. J. *Phys. Chem. Chem. Phys.* **2002**, *4*, 5937.

(21) Bässler, M.; Forsell, J.-O.; Björneholm, O.; Feifel, R.; Jurvansuu, M.; Aksela, S.; Sundin, S.; Sorensen, S. L.; Nyholm, R.; Ausmees, A.; Svensson, S. *J. Electron Spectrosc. Relat. Phenom.* **1999**, *101*, 953.

(22) (a) Coville, M.; Thomas, T. D. *Phys. Rev. A* **1991**, *43*, 6053. (b) Campbell, J. L.; Papp, T. *Atomic Data Nuclear Data Tables* **2001**, *77*, 1.

(23) Cavalleri, M.; Odelius, M.; Nilsson, A.; Pettersson, L. G. M. *J. Chem. Phys.* **2004**, *121*, 10065.

(24) Triguero, L.; Plashkevych, O.; Pettersson, L. G. M.; Ågren, H. *J. Electron Spectrosc. Relat. Phenom.* **1999**, *104*, 195.

(25) Triguero, L.; Petersson, L. G. M.; Ågren, H. *Phys. Rev. B* **1998**, *58*, 8057.

(26) Domcke, W.; Cederbaum, L. S. *J. Chem. Phys.* **1977**, *60*, 2878.

(27) Cederbaum, L. S. *J. Chem. Phys.* **1995**, *103*, 562.

(28) Sundin, S.; Ausmees, A.; Sorensen, S. L.; Björneholm, O.; Hjelte, I.; Svensson, S. *J. Phys. B: At. Mol. Opt. Phys.* **1997**, *30*, L851.

(29) Frisch, M. J.; Trucks, G. W.; Schlegel, H. B.; Scuseria, G. E.; Robb, M. A.; Cheeseman, J. R.; Montgomery, J. A., Jr.; Vreven, T.; Kudin, K. N.; Burant, J. C.; Millam, J. M.; Iyengar, S. S.; Tomasi, J.; Barone, V.; Mennucci, B.; Cossi, M.; Scalmani, G.; Rega, N.; Petersson, G. A.; Nakatsuji, H.; Hada, M.; Ehara, M.; Toyota, K.; Fukuda, R.; Hasegawa, J.; Ishida, M.; Nakajima, T.; Honda, Y.; Kitao, O.; Nakai, H.; Klene, M.; Li, X.; Knox, J. E.; Hratchian, H. P.; Cross, J. B.; Adamo, C.; Jaramillo, J.; Gomperts, R.; Stratmann, R. E.; Yazyev, O.; Austin, A. J.; Cammi, R.; Pomelli, C.; Ochterski, J. W.; Ayala, P. Y.; Morokuma, K.; Voth, G. A.; Salvador, P.; Dannenberg, J. J.; Zakrzewski, V. G.; Dapprich, S.; Daniels, A. D.; Strain, M. C.; Farkas, O.; Malick, D. K.; Rabuck, A. D.; Raghavachari, K.; Foresman, J. B.; Ortiz, J. V.; Cui, Q.; Baboul, A. G.; Clifford, S.; Cioslowski, J.; Stefanov, B. B.; Liu, G.; Liashenko, A.; Piskorz, P.; Komaromi, I.; Martin, R. L.; Fox, D. J.; Keith, T.; Al-Laham, M. A.; Peng, C. Y.; Nanayakkara, A.; Challacombe, M.; Gill, P. M. W.; Johnson, B.; Chen, W.; Wong, M. W.; Gonzalez, C.; Pople, J. A. *Gaussian 03*, Revision B.03; Gaussian, Inc.: Pittsburgh PA, 2003.

(30) Helgaker, T.; Jensen, H. J. A.; Joergensen, P.; Olsen, J.; Ruud, K.; Ågren, H.; Auer, A. A.; Bak, K. L.; Bakken, V.; Christiansen, O.; Coriani, S.; Dahle, P.; Dalskov, E. K.; Enevoldsen, T.; Fernandez, B.; Haettig, C.; Hald, K.; Halkier, A.; Heiberg, H.; Hettema, H.; Jonsson, D.; Kirpekar, S.; Kobayashi, R.; Koch, H.; Mikkelsen, K. V.; Norman, P.; Packer, M. J.; Pedersen, T. B.; Ruden, T. A.; Sanchez, A.; Saue, T.; Sauer, S. P. A.; Schimmelpfennig, B.; Sylvester-Hvid, K. O.; Taylor, P. R.; Vahtras, O. *Dalton, a molecular electronic structure program*, Release 1.2; 2001; http://www.kjemi.uio.no/software/dalton.

(31) Gradients were calculated using the values of the core excited-state energies E_{exc} in three points: $\Delta Q_\alpha = 0$, 1.5, 3.0 a.u. $\sqrt{amu}$.

(32) Arulmozhiraja, S.; Fujii, T. *J. Chem. Phys.* **2001**, *115*, 10589.

(33) Göller, A.; Grummt, U.-W. *Chem. Phys. Lett.* **2000**, *321*, 399.

(34) Bastiansen, O.; Fernholt, L.; Cyvin, B. N.; Cyvin, S. J.; Samdal, S.; Almenningen, A. *J. Mol. Struct.* **1985**, *128*, 59.

(35) Samdal, S.; Bastiansen, O. *J. Mol. Struct.* **1985**, *128*, 115.

(36) Rubio, M.; Mechán, M.; Ort, E.; Roos, B. O. *Chem. Phys. Lett.* **1995**, *234*, 373.

(37) Caravetta, V.; Plashkevych, O.; Ågren, H. *Chem. Phys.* **2001**, *263*, 231.

(38) Gel'mukhanov, F.; Ågren, H. *J. Chem. Phys.* **1995**, *103*, 5848.

(39) Ågren, H.; Vahtras, O.; Caravetta, V. *Chem. Phys.* **1995**, *196*, 47.
(40) Furuya, K.; Torii, H.; Furukawa, Y.; Tasumi, M. *J. Mol. Struct. (THEOCHEM)* **1998**, *424*, 225.
(41) Gel'mukhanov, F.; Ågren, H. *J. Phys. B: At. Mol. Opt. Phys.* **1995**, *28*, 3699.
(42) Trofimov, A. B.; Gromov, E. V.; Köppel, H.; Schirmer, J.; Prince, K. C.; Richter, R.; de Simone, M.; Coreno, M. *J. Phys. B: At. Mol. Opt. Phys.* **2003**, *36*, 3805.
(43) Niu, B.; Shirley, D.; Bai, Y. *J. Chem. Phys.* **1993**, *98*, 4377.
(44) Dobrodey, N. V.; Köppel, H.; Cederbaum, L. S. *Phys. Rev. A* **1998**, *60*, 1988.
(45) We estimate that with our method of calculation the gradients of the potential-energy surface related to C−H modes are certainly too high, which leads to a slight overestimation of such modes. This is related to the very steep potential-energy surface and to the fact that the step width in the numerical differentiation procedure are kept constant.
(46) Ma, Y.; Sette, F.; Meigs, G.; Modesti, S.; Chen, C. T. *Phys. Scr.* **1990**, *41*, 833.